ACS Photonics

Article

pubs.acs.org/journal/apchd5

Plasmonic Multibowtie Aperture Antenna with Fano Resonance for Nanoscale Spectral Sorting

Yang Chen,[†] Jiaru Chu,*[,†] and Xianfan Xu*[,‡]

[†]Micro&Nano Engineering Lab, University of Science and Technology of China, Hefei City, Anhui Province 230026, China

[‡]School of Mechanical Engineering and Birck Nanotechnology Center, Purdue University, West Lafayette, Indiana 47907, United States

Supporting Information

ABSTRACT: In this work we report a new type of nanostructure, the plasmonic multibowtie aperture antenna with Fano resonance for spectral sorting at the nanoscale. Redistribution of surface current in our device plays a critical role in mode coupling to generate Fano resonance, which has never been carefully discussed before. Numerical analyses show that interactions of the electric field, the surface current, and the resulting magnetic field are all important for achieving the desired spectral sorting. Depending on the constructive or destructive interference between the broadband dipole mode and the narrow band multipole mode, electric near-field amplitude and phase distributions switch dramatically across the Fano resonance, which are observed in real space using transmission-type s-SNOM. Based on the Fano interference, photons ranging from visible to infrared spectrum can be sorted through different channels at the nanoscale according to their wavelengths, which shows apparent advantages over other existing nanoscale spectral sorters. Moreover, the narrow gap plasmonic bowtie aperture provides enhanced field of the sorted photons, thus, offers a new approach for multicolor photodetection, optical filtering, and advanced biosensing.

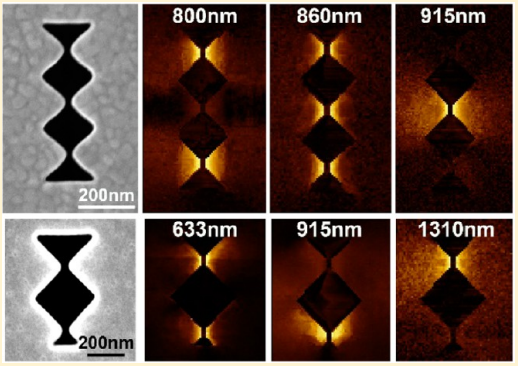

KEYWORDS: *Fano resonance, scanning near-field optical microscopy, surface plasmon, spectral sorting, near-field coupling, multipolar mode excitation*

Plasmonic nanostructures with ultrasharp Fano resonance have received considerable interests, since they can be applied in surface enhanced Raman spectroscopy (SERS),[1,2] biosensing,[3,4] and nonlinear optics.[5,6] Originating from quantum mechanics, Fano resonance is a general physical phenomenon found in systems with a broad continuum of energy level and a narrow band of states at the same energy. In purely plasmonic systems, a bright, superradiant plasmonic mode with a short lifetime spectrally overlaps with a dark, subradiant plasmonic mode with a long lifetime, resulting in Fano resonance with a non-Lorentzian line shape.[7−9]

Among various plasmonic nanostructures with Fano resonance, the particle-type nanostructures with multiple components arranged in designed patterns and separated by nanoscale gaps have been discussed most frequently, such as the dolmen structure,[10] the nonconcentric ring/disk cavity,[11] and the plasmonic oligomers.[12,13] The bright mode and the dark mode are coupled mainly through near-field interactions in the gaps and thus the field overlap between the two modes is critical for Fano resonance excitation.[14−16] Besides, the nanostructures composed of one single particle have also been studied before, such as the metallic nanodisk with a missing wedge[17] and the nonconcentric core−shell nanostructure.[18] In these works,[17−20] only the induced charge and electric field distributions are discussed to reveal the mechanism of Fano resonance generation. The situation can be different for the aperture-type nanostructures in a metal film, for which all metal parts are electrically connected. The induced surface current can therefore play an important role in Fano resonance excitation, which has never been carefully studied to our knowledge. We also demonstrate that the interactions of the electric field, the surface current, and the resulting magnetic field are all important for mode coupling in Fano resonance generation.

In this Letter, we report a novel plasmonic nanostructure named plasmonic multibowtie aperture antenna with Fano resonance. We will demonstrate that the induced surface current plays a critical role in coherent coupling between the bright dipole mode and the dark multipole mode. Scattering-type scanning near-field microscopy is used to visualize the amplitude and phase resolved electric near-field distribution of the structure, which was shown to be able to reveal Fano resonance. Consistent with the numerical simulation, the near-field intensity and phase patterns transform significantly across the Fano resonance as a result of the modulated Fano interference, which can achieve nanoscale spectral sorting from visible to infrared wavelengths. Incident photons are sorted and

Received: May 18, 2016
Published: August 1, 2016

DOI: 10.1021/acsphotonics.6b00345
ACS Photonics 2016, 3, 1689−1697

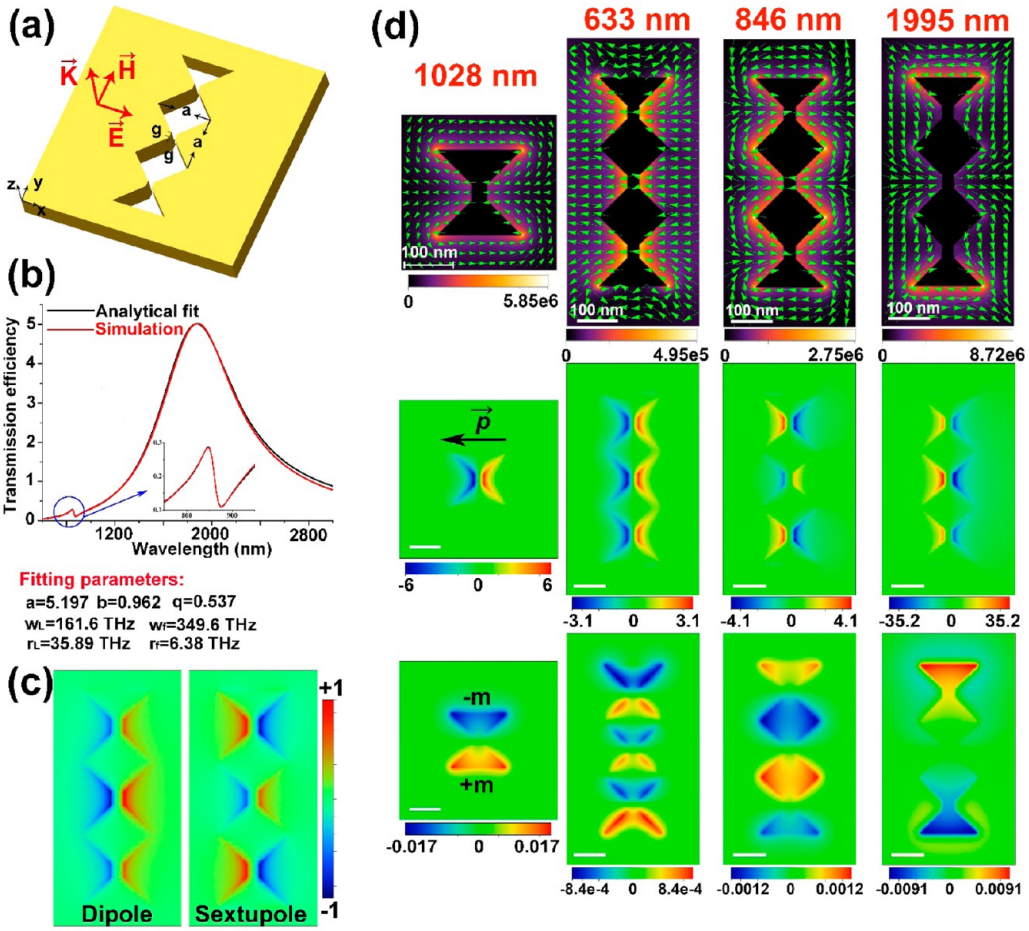

Figure 1. (a) Schematic of a triple-bowtie aperture structure. (b) FDTD simulated and analytical mode fitted transmission spectrum of the structure, the transmission efficiency is defined as transmitted intensity integrated over the aperture area normalized by the incident intensity integrated over the same area. (c) Charge distributions for the dipole mode and the sextupole mode. (d) Induced surface current $\vec{J}$ (row 1, the background brightness and field arrows, respectively, indicate the magnitude and direction of the surface current, unit: A/m^2), the real part of the longitudinal electric field component Re(E_z) (row 2, unit: V/m), and the real part of the longitudinal magnetic field component Re(H_z) (row 3, unit: A/m) distribution for a bowtie aperture at 1028 nm (column 1) and a triple-bowtie aperture at 633, 846, and 1995 nm (columns 2–4), these distributions are extracted at the exit plane, scale bar: 100 nm.

converged through different gaps of the multibowtie aperture according to their wavelengths. This new type of structure promises potential applications in color sensing,[21,22] spectroscopic detection,[23] biological separation,[24] and photonics metamaterials.[25,26]

RESULTS AND DISCUSSION

Plasmonic Interaction Analysis of the Triple-Bowtie Aperture Antenna. A typical plasmonic multibowtie aperture antenna shown in Figure 1a consists of three identical bowtie apertures (the outline dimension a = 170 nm and the gap g = 30 nm) connected end to end in a suspended gold film which can be fabricated using microfabrication methods. Calculating its transmission spectrum using the finite difference time domain method (Lumerical FDTD Solutions), we observe two transmission resonances as shown in Figure 1b: the Lorentzian symmetric resonance at 1995 nm and the non-Lorentzian asymmetric resonance at 846 nm.

To analyze its plasmonic states, we start from a single bowtie aperture in Figure 1d (column 1). With proper optical excitation, surface current arises from one ridge, flows around the aperture and ends on the opposite ridge, depositing electric charges with opposite signs on the two ridges. This current oscillates at the frequency of the incident light. Electric field is highly enhanced and localized in the gap area, and the magnetic field in the two arms oscillates out of phase. Therefore, the bowtie aperture can be considered as a combination of oscillating electric dipole $\vec{p}$ and two magnetic dipoles $\pm \vec{m}$. For a triple-bowtie aperture antenna, all three electric dipoles and six magnetic dipoles are coupled by the redistribution of surface current. At 633 nm, surface current starts from the same ridge of the three bowtie apertures and streams respectively toward the opposite ridge, resulting in three electric dipoles oscillating in phase just like a single dipole, corresponding to the dipole mode of the structure, as shown in Figure 1c. Coupling between the three component bowtie apertures is weak. At 846 nm, surface current originating from one ridge of the end bowtie aperture (the right ridge in Figure 1d) diverges into two branches: one flows around the aperture and ends at the opposite ridge, and the other flows toward the same ridge of the center aperture. Similarly, surface current originating from the left ridge of the center bowtie aperture flows partly to the opposite ridge of the same aperture and partly to the same ridge of the end bowtie apertures. In this way, the three electric dipoles are effectively coupled. The end electric dipoles oscillate in phase with each other and out of phase with the center

DOI: 10.1021/acsphotonics.6b00345
ACS Photonics 2016, 3, 1689–1697

dipole. In the Re(H_z) plot, adjacent magnetic dipoles of two connected bowtie apertures join into one, which further enhances the coupling effect. This resonance with asymmetric line shape is attributed to the Fano resonance resulting from the coherent interference between the bright dipole mode and the dark sextupole mode in which the end dipoles oscillate out of phase with the center dipole as shown in Figure 1c. The coupling between the two modes is mainly through the redistribution of the surface current as shown, and the fusion of the adjacent magnetic field also helps to enhance the mode coupling. At 1995 nm, the surface current arising from one ridge of the center aperture diverges, merges, respectively, with surface current arising from the same ridge of the two end apertures, steams around and terminates at the opposite ridges. As a result, the three individual electric dipoles oscillate in phase and the symmetric resonance is attributed to the dipole resonance. Based solely on the electric field distribution, it seems that the plasmonic interaction is the same for 1995 and 633 nm. But we can see from the surface current distribution and especially the magnetic field distribution that the three component bowtie apertures are strongly coupled at 1995 nm. The upper three magnetic dipoles fuse into one, and the same with the lower three magnetic dipoles. Across the end gap, there is some phase shift for the magnetic field due to the existence of an electric dipole there. Accordingly, aside from the electric field distribution, surface current and magnetic field distribution are also important to reveal the near-field interactions of the plasmonic nanostructure and the resulting spectral sorting behavior.

To further analyze the origin of the two resonances, we fit the transmission spectrum to the analytical model[14,27] described in eq 1.

$$T(\omega) = T_L(\omega) \times T_f(\omega) = \frac{a}{\left(\frac{\omega^2 - \omega_L^2}{2\gamma_L\omega_L}\right)^2 + 1} \times \frac{\left(\frac{\omega^2 - \omega_f^2}{2\gamma_f\omega_f} + q\right)^2 + b}{\left(\frac{\omega^2 - \omega_f^2}{2\gamma_f\omega_f}\right)^2 + 1} \quad (1)$$

This model was developed to analyze plasmonic Fano resonance. The Lorentzian function $T_L(w)$ describes the radiative contribution of the superradiant "bright" mode (here the dipole mode) while the non-Lorentzian envelope $T_f(w)$ represents the asymmetric modulation by the subradiant "dark" mode (here the sextupole mode) to generate the Fano resonance. The frequencies ω_L and ω_f indicate their resonance positions while the damping coefficients γ_L and γ_f indicate their resonance widths. The parameters q and b are, respectively, used to judge the asymmetry degree and modulation damping originating from intrinsic losses. As depicted in Figure 1b, the analytical model fits the simulated transmission spectrum well, testifying the nature of the two resonances. The quality factor of the Fano resonance is calculated to be 54.8.

Babinet's theory provides a unique perspective to reveal plasmonic interactions of the triple-bowtie aperture.[28−30] The diabolo triple-bowtie antenna, as the electromagnetic dual of the triple-bowtie aperture is shown in Figure 2a together with its illumination scheme. As depicted in Figure 2b, two resonances are observed in its extinction spectrum: the magnetic dipole resonance at 1962 nm and the Fano resonance at 828 nm, corresponding respectively to the dipole resonance and the Fano resonance of the triple-bowtie aperture. For the magnetic dipole resonance, surface current arising from the top bowtie flows straightforward to the bottom bowtie, producing

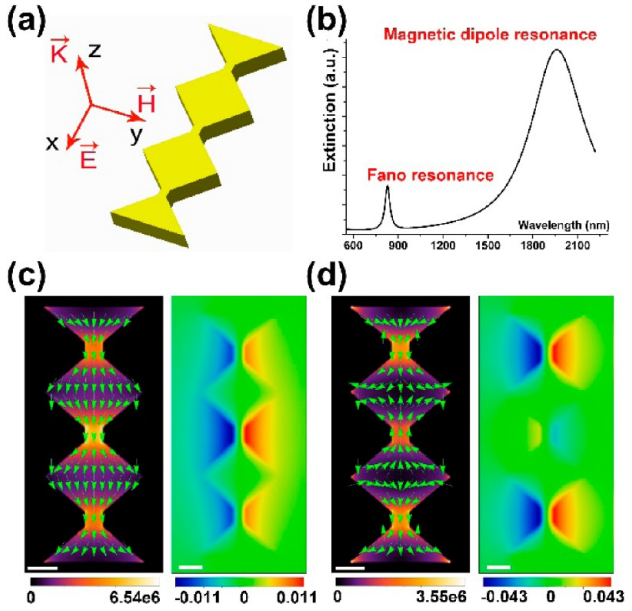

Figure 2. (a) Schematic of a diabolo triple-bowtie antenna. (b) Calculated extinction spectrum of the structure. (c, d) Induced surface current $\vec{J}$ (unit: A/m^2) and the real part of the longitudinal magnetic field component Re (H_z; unit: A/m) distribution at 1962 nm (c) and 828 nm (d) extracted on the upper surface; scale bar: 50 nm.

enhanced magnetic field azimuthally polarized around the three metal bridges, as shown in Figure 2c. Its Re (H_z) plot has a distribution pattern similar to the Re (E_z) plot of the triple-bowtie aperture at its dipole resonance. For the Fano resonance, the surface current of the center bowtie propagates in the opposite direction relative to that of the two end bowties, resulting in magnetic field with inverse polarization there as shown in Figure 2d. Based on its Re (H_z) plot, this resonance is attributed to the coherent interference between the bright magnetic dipole mode and the dark magnetic sextupole mode.

Experimental Measurements and Numerical Simulations of the Near-Field Distribution. Transmission-type s-SNOM is utilized to simultaneously observe the near-field amplitude $|E_z|$ and the phase φ_z and, also, the topography of the sample. Plane wave illumination with proper polarization is employed from below the sample. Light scattered by a dielectric Si tip located above the sample is collected and analyzed using higher-harmonic demodulation[31] and pseudoheterodyne interferometry.[32] Multiple laser sources with distinct wavelengths ranging from 633 to 1550 nm are installed and switched during experiments.

As shown in Figure 3e, the superradiant dipole mode is solely excited far from the Fano resonance at 633 and 1550 nm, which is most apparent in the phase images where all the three dipoles oscillate in phase with each other. At the gap of each aperture, charges with opposite signs accumulate at apexes of the two closely spaced metal tips, acting just like a dipole, producing highly enhanced and localized electric field there. Thus, we observe two adjacent hotspots on each side of the gap in $|E_z|$ and a phase jump of π across the gap in φ_z.[33] Around the Fano resonance, the sextupole mode is also excited and interferes with the dipole mode mainly through the redistribution of surface current as described before. Depending on the relative amplitude and phase-shift of the two modes, the near-field amplitude and phase distribution change significantly with the wavelength. The near-field amplitude at 860 nm is almost the

DOI: 10.1021/acsphotonics.6b00345
ACS Photonics 2016, 3, 1689−1697

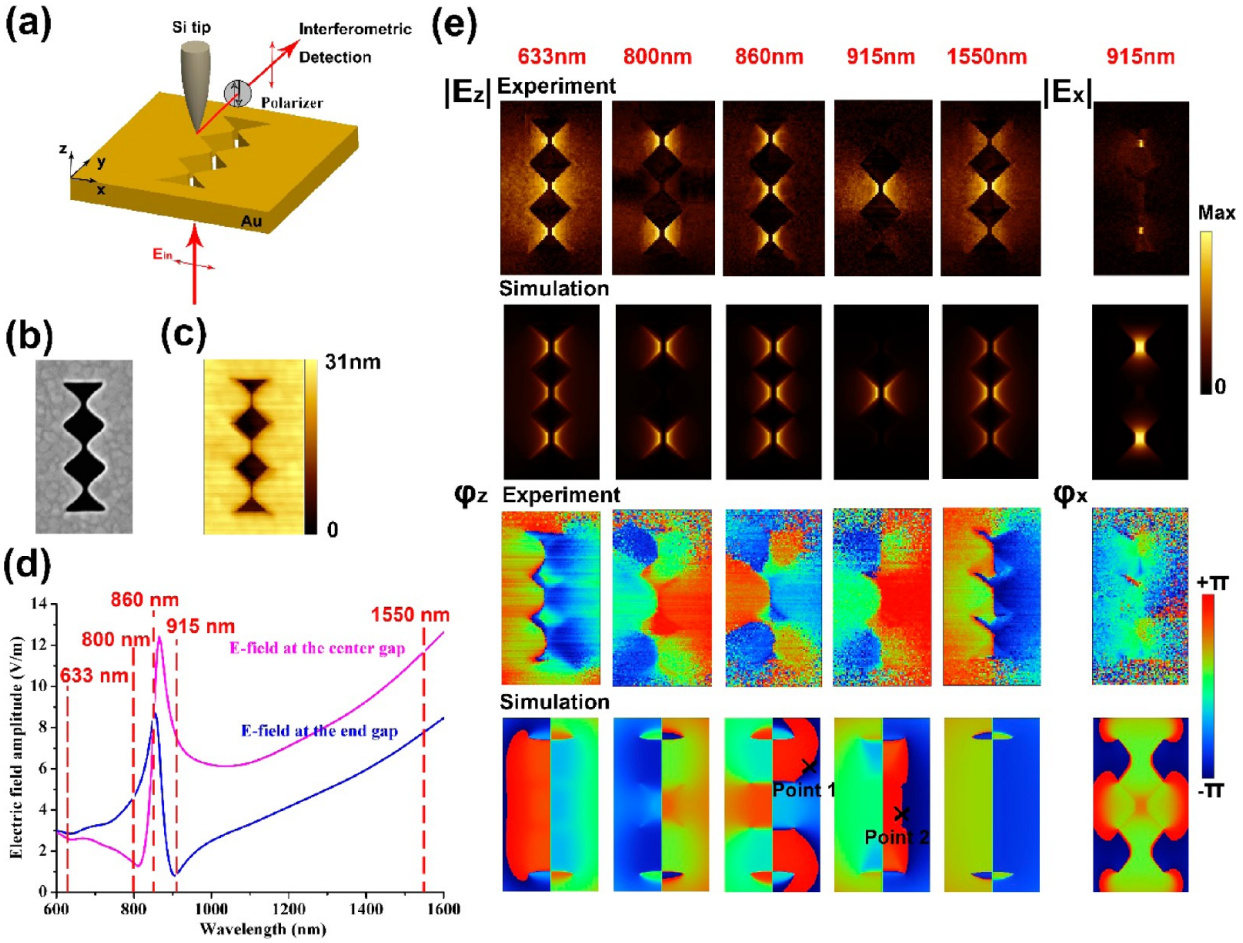

Figure 3. (a) Experimental setup for near-field mapping in transmission mode. (b) SEM image of the triple-bowtie aperture sample. (c) Topography of the sample measured by AFM. (d) Calculated electric field amplitude at the center gap and the end gap. (e) Experimental and calculated near-field amplitude and phase distribution of E_x and E_z at distinct wavelengths (image size of SEM, AFM, and s-SNOM: 360 nm × 660 nm).

same with that at 633 nm, where all the three dipoles are excited with similar intensity. However, its near-field phase image presents a phase shift of 2.81 rad for the central dipole relative to the end dipole, demonstrating that the sextupole mode dominates over the dipole mode at this wavelength. At 800 nm, only the end dipoles are excited, because the interference is highly destructive for the central gap. This near-field pattern is reversed at 915 nm for the heavily destructive interference at the end gaps. Important to note that the phase jump at points 1 and 2 indicated in the phase image is 2π, which is caused by the plot range of the software. In fact, the phase is continuous there. The magnetic field and surface current distribution at 800 and 915 nm as hybridization of the two modes can be found in Supporting Information, Figure 5a. The transverse component of the electric field $|E_x|$ and φ_x can also be measured. As shown in Figure 3e (column 6), the two end dipoles are excited at 915 nm, while the central dipole is strongly suppressed due to the destructive interference. Different from the longitudinal component E_z, only one intense hotspot is observed for $|E_x|$ in each excited gap and the phase signal is continuous across the gap.

Spectral Sorting Performance and Phase Difference Analysis. The unique near-field property described above is exploited for nanoscale spectral sorting. To evaluate the spectral sorting or filtering performance of the structure, a filtering ratio (FR) is introduced as

$$\mathrm{FR}_{i-j} = \left(\frac{|E_i|}{|E_j|}\right)^2 \tag{2}$$

where $|E_i|$ and $|E_j|$ are the electric field amplitudes detected at different gaps. The reason for such a definition is discussed in the Supporting Information. The subscripts i and j indicate the position of the gap (i.e., end vs center). As shown in Figure 4a, the simulation result gives the largest $\mathrm{FR}_{\mathrm{end-center}}$ of 101 at 788 nm and the largest $\mathrm{FR}_{\mathrm{center-end}}$ of 102 at 900 nm, which is better than the existing nanoscale spectral sorters.[21,34,35] The experimental data matches well with the simulated results. Power flow images in Figure 4c clearly depict that incoming photons at 800 nm are converged and transmitted through the two end gaps and are completely blocked by the central gap. In contrary, incident photons at 915 nm are selectively focused through the central gap. The phase difference between the central and the end gaps plotted in Figure 4b provides further insights into the Fano resonance. The difference is 0 for the dipole mode and π for the sextupole mode. Due to the superposition of the two modes, the resulting phase difference could have any value between 0 and π based on their relative excitation magnitudes.[36,37] At 832 nm, the phase difference reaches its maximum value of 2.73 rad because the dark sextupole mode is dominant there. The absolute phase difference of the dark mode π cannot be obtained because the broadband dipole mode is always excited to a certain extent.

DOI: 10.1021/acsphotonics.6b00345
ACS Photonics 2016, 3, 1689−1697

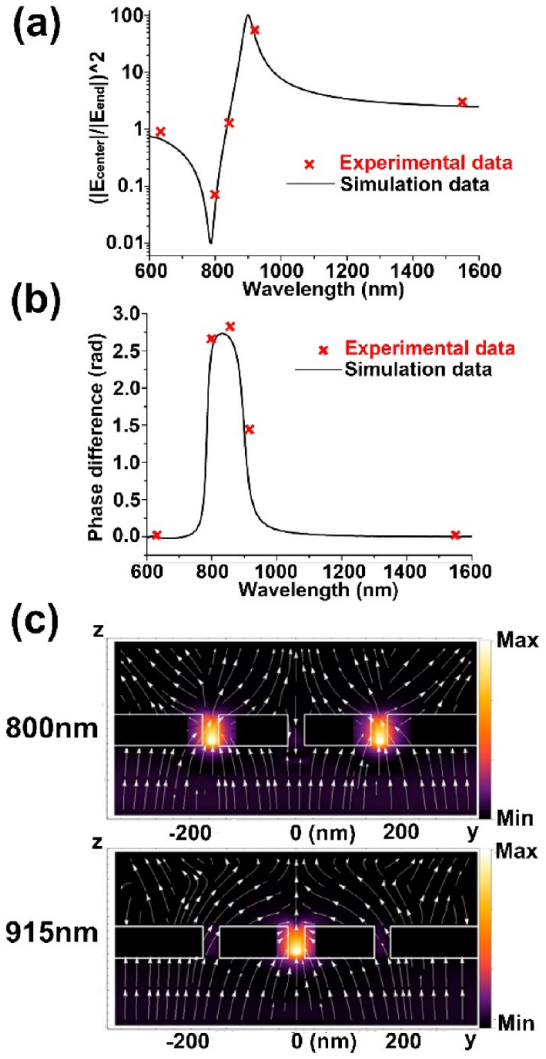

Figure 4. (a) Ratio between electric field intensity of the central gap and the end gap as a function of the wavelength, the y-coordinate is plotted in the log scale. (b) Electric field phase difference between the central and the end gap. (c) Calculated power flow on the $y-z$ plane at 800 and 915 nm.

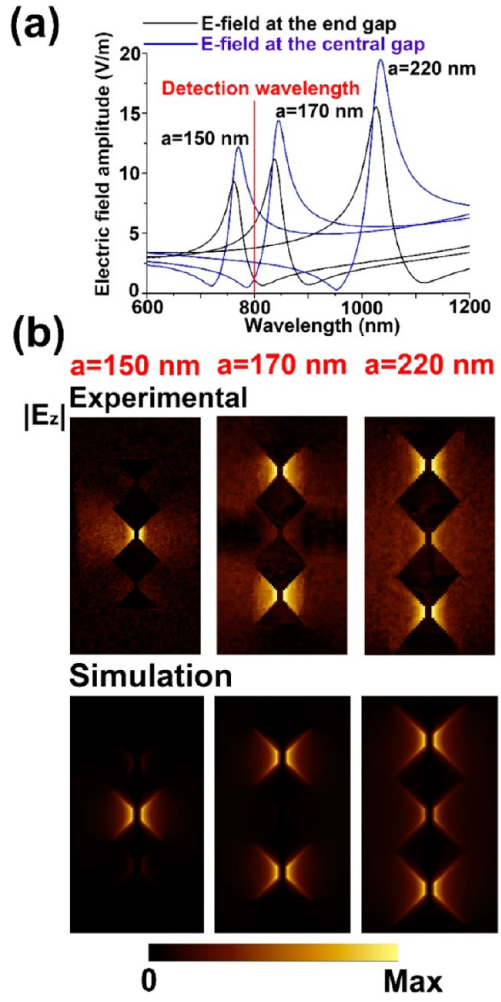

Figure 5. (a) Calculated electric field amplitude at the central and the end gap for different aperture size. (b) Experimental and simulated electric field amplitude distribution $|E_z|$ for different aperture size measured at 800 nm (Image size: 400 nm × 700 nm).

Away from the maximum position, the sextupole mode decays rapidly and the phase difference decreases to zero for which only the dipole mode is excited.

Tuning the Fano Resonance. We have demonstrated that photons with different energy can be sorted through different channels of a triple-bowtie aperture. Moreover, photons with the same energy can be filtered through different channels by adjusting the size of the structure as depicted in Figure 5. Larger aperture leads to a redshift of the Fano resonance, because both the dipole mode and the sextupole mode are redshifted.[38] Our experimental results agree well with simulations. Therefore, it is possible to design and fabricate nanoscale spectral sorters to filter photons with specific wavelength ranging from visible to infrared spectrum through a specified channel.

Plasmonic Interaction Analysis of the Asymmetric Double-Bowtie Aperture Antenna. When a double-bowtie aperture composed of two identical bowtie apertures is illuminated vertically, we can only observe a symmetric dipole resonance in the transmission spectrum. To break the symmetry, oblique illumination can be an effective strategy.[34] Alternatively, we can use two apertures with different structure parameters as shown in Figure 6a. Two transmission resonances are observed: one corresponds to the Lorentzian dipole resonance at 1690 nm and the other corresponds to the Fano resonance at 955 nm resulting from the interference between the superradiant dipole mode and the subradiant quadrupole mode. Figure 6c shows the charge distributions of the two modes. Comprehensive analysis of the electric field, magnetic field and surface current gives a complete picture of its plasmonic states as shown in Figure 6c. At 633 nm, the two bowtie apertures are weakly coupled. At the dipole resonance 1690 nm, the two individual electric dipoles oscillate in phase and the lower three magnetic dipoles combine into one. The surface current originating from one ridge of the upper aperture flows successively through the two ridges of the lower aperture and ends at its opposite ridge. At the Fano resonance 955 nm, the surface current arising from one ridge of the lower aperture flows partly toward the opposite ridge and partly toward the same ridge of the upper aperture, leading to the two electric dipoles oscillating out of phase. The two center magnetic dipoles fuse into one. We can see that the coupling between the dipole mode and the quadrupole mode is mainly through the redistribution of surface current. The analytical mode expressed in eq 1 fits the simulation result as shown in Figure 6b, which

DOI: 10.1021/acsphotonics.6b00345
ACS Photonics 2016, 3, 1689−1697

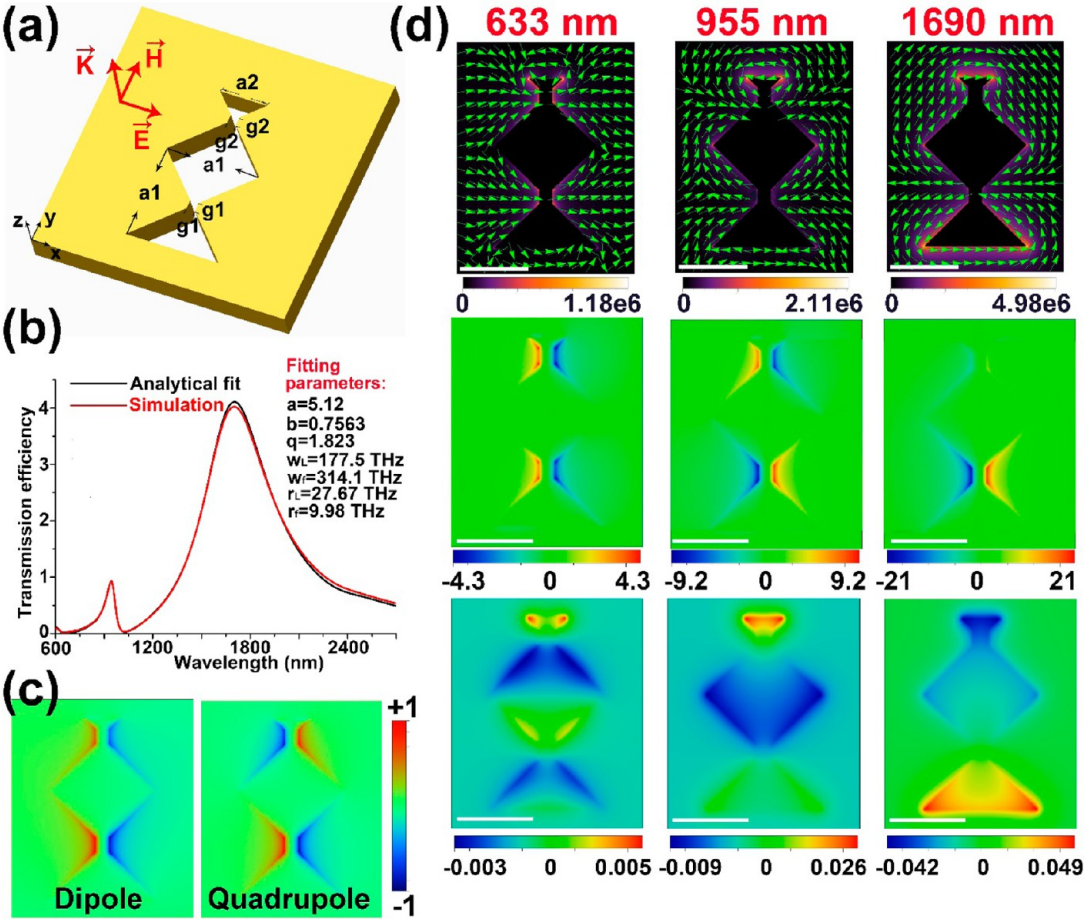

Figure 6. (a) Schematic of the asymmetric double-bowtie aperture. (b) FDTD simulated and analytical mode fitted transmission spectrum of the structure. (c) Charge distributions for the dipole mode and the quadrupole mode. (d) Induced surface current $\vec{J}$ (row 1, unit: A/m^2), the real part of the longitudinal electric field component Re(E_z) (row 2, unit: V/m), and the real part of the longitudinal magnetic field component Re(H_z) (row 3, unit: A/m) distribution for an asymmetric double-bowtie aperture at 633, 955, and 1690 nm (columns 1−3), these distributions are extracted at the exit plane; scale bar: 200 nm.

confirms the origin of the two resonances. The quality factor of the Fano resonance is calculated to be 31.5.

Spectral Sorting Performance and Phase Analysis of the Asymmetric Double-Bowtie Aperture Antenna. Around the Fano resonance, the near-field amplitude $|E_z|$ and phase φ_z distribution changes significantly as demonstrated by s-SNOM experiments and FDTD simulations in Figure 7d. At 915 nm, the interference is highly destructive at the upper gap, thus only the lower dipole is excited. The near-field amplitude pattern is inverted at 1310 nm, because the interference is destructive at the lower gap. The redistributed surface current and magnetic field at 915 and 1310 nm shown in Supplementary Figure 4a illustrate their critical role to enable nanoscale spectral sorting. Considering the spectral sorting performance as shown in Figure 7b, $FR_{lower-upper}$ reaches its maximum value of 17.5 at 908 nm, and $FR_{upper-lower}$ gets its maximum value of 917 at 1254 nm. Therefore, relative to the triple-bowtie aperture, the asymmetric double-bowtie aperture is more suitable to sort photons through the upper channel. Phase information provides further insights into the Fano interference, as depicted in Figure 7c. At 633 and 1550 nm, far from the Fano resonance, only the dipole mode is excited, and the lower and the upper dipole oscillate in phase. At 915 nm, the phase shift between the two dipoles is measured to be 1.56 rad, thus the quadrupole mode is excited and has comparative intensity with the dipole mode. In the wavelength range from 1020 to 1170 nm, the phase shift is calculated to exceed 2.7 rad, which suggests that the quadrupole mode dominates over the dipole mode. Comparing the phase difference curve of the triple-bowtie aperture and the asymmetric two-bowtie aperture, we can see that higher-order multipole mode has narrower resonance width, which means less radiative loss and longer decay time.[15]

Many of the existing nanostructures for spectral sorting consist of multiple separated components with different resonant wavelengths.[21,39−41] In contrast to them, our structure is much more compact and can sort photons in nanoscale. Note that our structure is not designed for sorting photons over large distance. Compared with the other two nanoscale spectral sorters, the Anti-Hermitian coupling of an array of gold antennas[35] and the double-nanogap structure,[34] our structure can effectively suppress the background illumination, leading to a much better filtering ratio, which is the critical parameter to judge the spectral sorting performance. Also, the quality factor of the Fano resonance in our structure is larger than the other two. However, our structure has a smaller electric field enhancement relative to the other two structures owning to its relatively weaker Fano resonance, which is worth further improvement. Overall, our structure is a better candidate for nanoscale spectral sorting.

DOI: 10.1021/acsphotonics.6b00345
ACS Photonics 2016, 3, 1689−1697

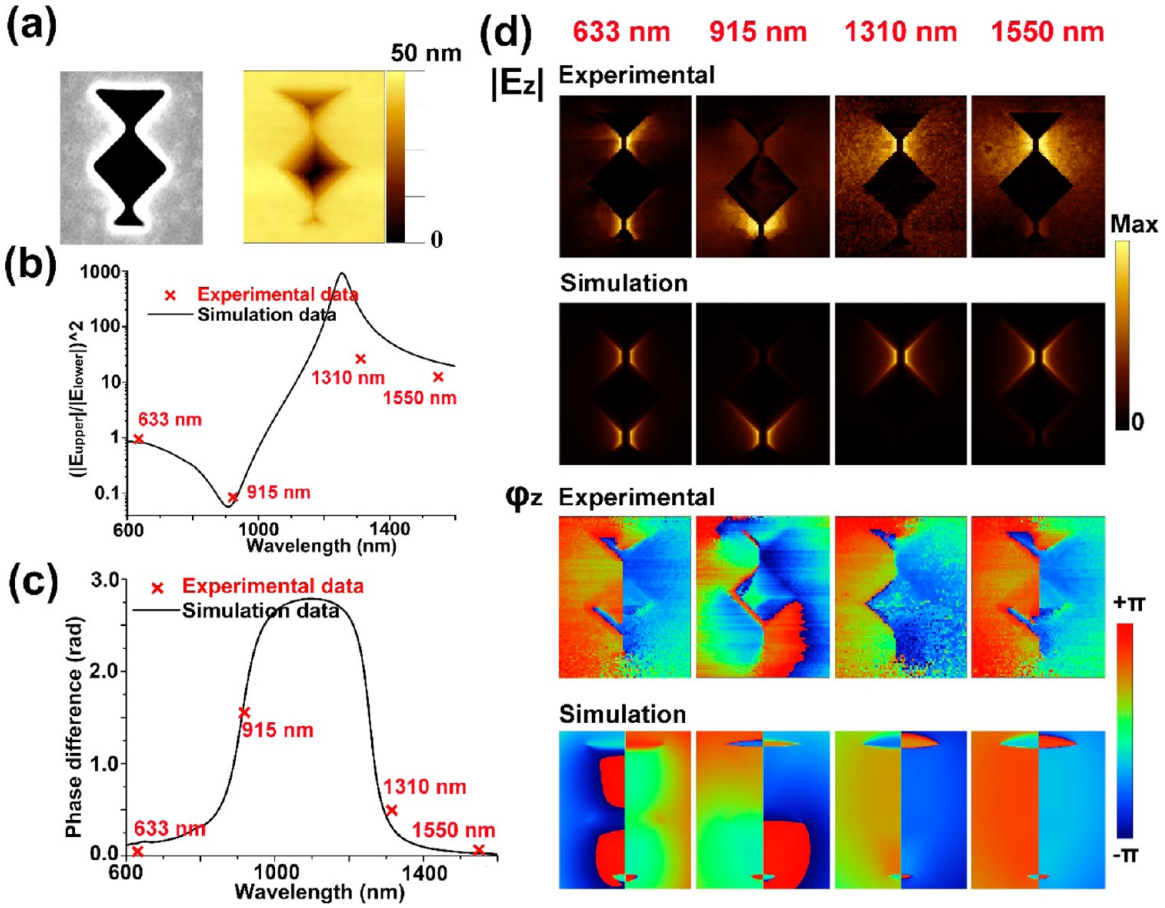

Figure 7. (a) SEM and AFM of the sample. (b) Calculated filtering ratio (FR), the *y*-coordinate is plotted in the log scale. (c) Phase difference between the upper and the lower dipole. (d) Calculated and experimental near-field amplitude $|E_z|$ and phase φ_z distribution at wavelengths indicated in (c). Image size of SEM, AFM, and s-SNOM: 540 nm × 640 nm.

CONCLUSION

We presented plasmonic multibowtie aperture antenna with Fano resonance which can be used for nanoscale spectral sorting. Different from the particle-type plasmonic antennas, the redistribution of surface current is shown to be the key for the coupling between the bright mode and the dark mode. Using transmission-type s-SNOM, it was found that across the Fano resonance, the near-field amplitude and phase distribution changed dramatically, which was resulted from the interference between the "bright" dipole mode and the "dark" multipole mode. The experimental results agreed well with the simulation. Due to the interference at the gap, constructive or destructive, photons were selectively transmitted or blocked. Using different structural parameters of the multibowtie aperture, we can shift its Fano resonance and sort out photons with specific energy from a certain channel, which promises potential applications in color-sensitive photodetectors, multiplexed chemical sensing, biological separation, and photonics metamaterials.

METHODS

Sample Fabrication. The detailed sample fabrication process is shown in Supporting Information, Figure 2a. A SiO_2 film (thickness: 2 μm) and a Si_3N_4 film (thickness: 300 nm) are deposited, respectively, on the two sides of the Si wafer (thickness: 300 μm) using PECVD (Oxford System 100). Then a window (300 μm × 1 μm) is patterned by photolithography (SUSS MABA6), and the SiO_2 film in the window is removed by reactive ion etching (Oxford NGP80). After that, the bulk Si in the window is removed by inductively coupled plasma etching (Oxford ICP380) and KOH wet etching. Then, a layer of gold (thickness: 80 nm) is deposited on the Si_3N_4 film by E-beam evaporation (Lesker LAB18). Then the Si_3N_4 layer is etched out using FIB milling (FEI Helios 650, 30KV, 9.3 nA) with an end point detector, leaving the gold film suspended. Lastly, we perforate multibowtie apertures on the gold film using FIB (30KV, 1.1pA) with fabrication resolution of 2 nm. In this work, the apertures are milled in a suspended gold film, because the existence of underlying substrate with high refractive index will red-shift the Fano resonance and weaken the near-field intensity,[42] as shown in Supporting Information, Figure 2b. Moreover, surface plasmon resonance is apparently broadened by the substrate, and its quality factor is degraded.

Shown in Supporting Information, Figure 3a is an SEM image of a fabricated triple-bowtie aperture array in a suspended gold film. The suspended gold film has apparent contrast relative to the surrounding Si_3N_4 substrate, because it has much larger secondary electron yield. Supporting Information, Figure 3c shows a double-bowtie aperture array demonstrating excellent fabrication consistence. Supporting Information, Figure 3b and d are, respectively, the amplified SEM images of the triple-bowtie aperture and the double-bowtie aperture described in the main text.

Numerical Simulations and Analytical Fitting. Numerical simulations in this work are conducted using commercial

DOI: 10.1021/acsphotonics.6b00345
ACS Photonics 2016, 3, 1689−1697

finite difference time domain software (Lumerical FDTD Solutions). Optical properties of gold is taken from Palik.[43] A broadband plane wave with electric component of 1 V/m and magnetic component of 0.00253 A/m is used and the polarization is set to be across the gap. 1 nm × 1 nm × 1 nm mesh size is used in the aperture area to maintain the simulation accuracy. The fitting of the transmission spectrum using the analytical model described in eq 1 is done by the *cftool* package of Matlab.

Transmission-Mode s-SNOM for Near-Field Mapping. As shown in Supporting Information, Figure 4, the transmission-mode s-SNOM is based on an AFM working in tapping mode. Excitation laser is incident upward on the sample with electric polarization across the gap. Multiple laser diodes with different wavelengths are installed and switched during experiments. The near field scattered by the dielectric Si tip is collected and directed to a photodetector. The tip we use is a commercial Si probe (Arrow-NCR, Nanoworld) to avoid plasmonic coupling between the tip and the sample.[44] The radius of the tip apex is 10 nm to achieve high resolution and the oscillation amplitude is 60 nm in our experiments. Higher harmonic demodulation and pseudoheterodyne interferometer are used to extract amplitude and phase signal from background. By adjusting the half-wave plate in the interferometric path and the polarizer in front of the detector, we can get near-field distribution of two orthogonal components E_p and E_s, which correspond to E_z and E_x in our experiments.[31,45]

■ ASSOCIATED CONTENT

Supporting Information

The Supporting Information is available free of charge on the ACS Publications website at DOI: 10.1021/acsphotonics.6b00345.

The basis of the definition of filter ratio; schematic of the sample fabrication process; influence of the substrate on electric field amplitude; SEM images of fabricated sample; schematic of the transmission-mode s-SNOM system; surface current, electric field and magnetic field distribution of the triple-bowtie aperture at 800 and 915 nm and the asymmetric double-bowtie aperture at 915 and 1310 nm (PDF).

■ AUTHOR INFORMATION

Corresponding Authors

*E-mail: jrchu@ustc.edu.cn.
*E-mail: xxu@ecn.purdue.edu.

Notes

The authors declare no competing financial interest.

■ ACKNOWLEDGMENTS

Y.C. and J.C. acknowledge financial support from the National Basic Research Program of China (973 Program, No.2011CB302101). X.X. acknowledges the support from the U.S. National Science Foundation (Grant No. CMMI-1462622). Sample fabrication and the s-SNOM scans are carried out in USTC Center for Micro- and Nanoscale Research and Fabrication.

■ REFERENCES

(1) Xu, H.; Bjerneld, E. J.; Käll, M.; Börjesson, L. Spectroscopy of Single Hemoglobin Molecules by Surface Enhanced Raman Scattering. *Phys. Rev. Lett.* **1999**, *83*, 4357−4360.

(2) Ye, J.; Wen, F.; Sobhani, H.; Lassiter, J. B.; Dorpe, P. V.; Nordlander, P.; Halas, N. J. Plasmonic nanoclusters: near field properties of the Fano resonance interrogated with SERS. *Nano Lett.* **2012**, *12*, 1660−1667.

(3) Anker, J. N.; Paige, H.; Olga, L.; Shah, N. C.; Jing, Z.; Duyne, R. P.; Van. Biosensing with plasmonic nanosensors. *Nat. Mater.* **2008**, *7*, 442−53.

(4) Chihhui, W.; Khanikaev, A. B.; Ronen, A.; Nihal, A.; Ahmet Ali, Y.; Hatice, A.; Gennady, S. Fano-resonant asymmetric metamaterials for ultrasensitive spectroscopy and identification of molecular monolayers. *Nat. Mater.* **2011**, *11*, 69−75.

(5) Zhang, Y.; Wen, F.; Zhen, Y.-R.; Nordlander, P.; Halas, N. J. Coherent Fano resonances in a plasmonic nanocluster enhance optical four-wave mixing. *Proc. Natl. Acad. Sci. U. S. A.* **2013**, *110*, 9215−9219.

(6) Thyagarajan, K.; Butet, J. r. m.; Martin, O. J. Augmenting second harmonic generation using Fano resonances in plasmonic systems. *Nano Lett.* **2013**, *13*, 1847−1851.

(7) Fano, U. Effects of Configuration Interaction on Intensities and Phase Shifts. *Phys. Rev.* **1961**, *124*, 1866−1878.

(8) Faist, J.; Capasso, F.; Sirtori, C.; West, K. W.; Pfeiffer, L. N. Controlling the sign of quantum interference by tunnelling from quantum wells. *Nature* **1997**, *390*, 589−591.

(9) Kroner, M.; Govorov, A. O.; Remi, S.; Biedermann, B.; Seidl, S.; Badolato, A.; Petroff, P. M.; Zhang, W.; Barbour, R.; Gerardot, B. D. The nonlinear Fano effect. *Nature* **2008**, *451*, 311−4.

(10) Verellen, N.; Sonnefraud, Y.; Sobhani, H.; Hao, F.; Moshchalkov, V. V.; Dorpe, P. V.; Nordlander, P.; Maier, S. A. Fano resonances in individual coherent plasmonic nanocavities. *Nano Lett.* **2009**, *9*, 1663−1667.

(11) Hao, F.; Sonnefraud, Y.; Dorpe, P. V.; Maier, S. A.; Halas, N. J.; Nordlander, P. Symmetry breaking in plasmonic nanocavities: subradiant LSPR sensing and a tunable Fano resonance. *Nano Lett.* **2008**, *8*, 3983−3988.

(12) Mirin, N. A.; Bao, K.; Nordlander, P. Fano resonances in plasmonic nanoparticle aggregates†. *J. Phys. Chem. A* **2009**, *113*, 4028−4034.

(13) Fan, J. A.; Chihhui, W.; Kui, B.; Jiming, B.; Rizia, B.; Halas, N. J.; Manoharan, V. N.; Peter, N.; Gennady, S.; Federico, C. Self-assembled plasmonic nanoparticle clusters. *Science* **2010**, *328*, 1135−8.

(14) Benjamin, G.; Martin, O. J. F. Influence of electromagnetic interactions on the line shape of plasmonic Fano resonances. *ACS Nano* **2011**, *5*, 8999−9008.

(15) Andrea, L.; Benjamin, G.; Peter, N.; Martin, O. J. F. Mechanisms of Fano resonances in coupled plasmonic systems. *ACS Nano* **2013**, *7*, 4527−4536.

(16) Hentschel, M.; Saliba, M.; Vogelgesang, R.; Giessen, H.; Alivisatos, A. P.; Liu, N. Transition from isolated to collective modes in plasmonic oligomers. *Nano Lett.* **2010**, *10*, 2721−2726.

(17) Fang, Z.; Cai, J.; Yan, Z.; Nordlander, P.; Halas, N. J.; Zhu, X. Removing a wedge from a metallic nanodisk reveals a Fano resonance. *Nano Lett.* **2011**, *11*, 4475−4479.

(18) Zhang, J.; Zayats, A. Multiple Fano resonances in single-layer nonconcentric core-shell nanostructures. *Opt. Express* **2013**, *21*, 8426−8436.

(19) Kraft, M.; Luo, Y.; Maier, S.; Pendry, J. Designing plasmonic gratings with transformation optics. *Phys. Rev. X* **2015**, *5*, 031029.

(20) Luo, Y.; Lei, D. Y.; Maier, S. A.; Pendry, J. B. Transformation-optics description of plasmonic nanostructures containing blunt edges/corners: from symmetric to asymmetric edge rounding. *ACS Nano* **2012**, *6*, 6492−6506.

(21) Laux, E.; Genet, C.; Skauli, T.; Ebbesen, T. W. Plasmonic photon sorters for spectral and polarimetric imaging. *Nat. Photonics* **2008**, *2*, 161−164.

(22) King, N. S.; Liu, L.; Yang, X.; Cerjan, B.; Everitt, H. O.; Nordlander, P.; Halas, N. J. Fano Resonant Aluminum Nanoclusters

DOI: 10.1021/acsphotonics.6b00345
ACS Photonics 2016, 3, 1689−1697

for Plasmonic Colorimetric Sensing. *ACS Nano* **2015**, *9*, 10628−10636.
(23) Zheng, B. Y.; Wang, Y.; Nordlander, P.; Halas, N. J. Color-Selective and CMOS-Compatible Photodetection Based on Aluminum Plasmonics. *Adv. Mater.* **2014**, *26*, 6318−6323.
(24) Chaumet, P. C.; Adel, R. Optical tweezers: dressed for success. *Nat. Nanotechnol.* **2014**, *9*, 252−3.
(25) Yu, N.; Capasso, F. Flat optics with designer metasurfaces. *Nat. Mater.* **2014**, *13*, 139−50.
(26) Meinzer, N.; Barnes, W. L.; Hooper, I. R. Plasmonic meta-atoms and metasurfaces. *Nat. Photonics* **2014**, *8*, 889−898.
(27) Chen, Y.; Martin, O. J. F. Periodicity-induced symmetry breaking in a Fano lattice: hybridization and tight-binding regimes. *ACS Nano* **2014**, *8*, 11860−11868.
(28) Born, M.; Wolf, E. *Principles of Optics*, 7th ed.; Pergamon Press, 1980; pp 1188−1189.
(29) Zentgraf, T.; Meyrath, T. P.; Seidel, A.; Kaiser, S.; Giessen, H. Babinet's principle for optical frequency metamaterials and nanoantennas. *Phys. Rev. B: Condens. Matter Mater. Phys.* **2007**, *76*, 3407.
(30) Yang, H. U.; Olmon, R. L.; Deryckx, K. S.; Xu, X. G.; Bechtel, H. A.; Xu, Y.; Lail, B. A.; Raschke, M. B. Accessing the optical magnetic near-field through Babinet's principle. *ACS Photonics* **2014**, *1*, 894−899.
(31) Hillenbrand, R.; Keilmann, F. Complex optical constants on a subwavelength scale. *Phys. Rev. Lett.* **2000**, *85*, 3029−32.
(32) Ocelic, N.; Huber, A.; Hillenbrand, R. Pseudoheterodyne detection for background-free near-field spectroscopy. *Appl. Phys. Lett.* **2006**, *89*, 101124.
(33) Chen, Y.; Chen, J.; Xu, X.; Chu, J. Fabrication of bowtie aperture antennas for producing sub-20 nm optical spots. *Opt. Express* **2015**, *23*, 9093−9099.
(34) Tanaka, Y. Y.; Komatsu, M.; Fujiwara, H.; Sasaki, K. Nanoscale Color Sorting of Surface Plasmons in a Double-Nanogap Structure with Multipolar Plasmon Excitation. *Nano Lett.* **2015**, *15*, 7086−90.
(35) Zhang, S.; Ye, Z.; Wang, Y.; Park, Y.; Bartal, G.; Mrejen, M.; Yin, X.; Zhang, X. Anti-Hermitian plasmon coupling of an array of gold thin-film antennas for controlling light at the nanoscale. *Phys. Rev. Lett.* **2012**, *109*, 193902.
(36) Alzar, C. L. G.; Martinez, M. A. G.; Nussenzveig, P. Classical Analog of Electromagnetically Induced Transparency. *Am. J. Phys.* **2002**, *70*, 37−41.
(37) Alonsogonzalez, P.; Schnell, M.; Sarriugarte, P.; Sobhani, H.; Wu, C.; Arju, N.; Khanikaev, A.; Golmar, F.; Albella, P.; Arzubiaga, L. Real-Space Mapping of Fano Interference in Plasmonic Metamolecules. *Nano Lett.* **2011**, *11*, 3922−3926.
(38) Novotny, L.; Hecht, B.; Keller, O. *Principles of Nano-Optics*; Cambridge University Press, 2012; p 41.
(39) Xu, T.; Wu, Y.-K.; Luo, X.; Guo, L. J. Plasmonic nanoresonators for high-resolution colour filtering and spectral imaging. *Nat. Commun.* **2010**, *1*, 59.
(40) Yokogawa, S.; Burgos, S. P.; Atwater, H. A. Plasmonic color filters for CMOS image sensor applications. *Nano Lett.* **2012**, *12*, 4349−4354.
(41) Ellenbogen, T.; Seo, K.; Crozier, K. B. Chromatic plasmonic polarizers for active visible color filtering and polarimetry. *Nano Lett.* **2012**, *12*, 1026−1031.
(42) Otte, M. A.; Estévez, M. C.; Carrascosa, L. G.; Gonzálezguerrero, A. B.; Lechuga, L. M.; Sepúlveda, B. Improved Biosensing Capability with Novel Suspended Nanodisks. *J. Phys. Chem. C* **2011**, *115*, 5344−5351.
(43) Palik, E. D. Handbook of optical constants of solids. *Academic Press Handbook* **1985**, *33*, 189.
(44) Esteban, R.; Vogelgesang, R.; Kern, K. Tip-substrate interaction in optical near-field microscopy. *Phys. Rev. B: Condens. Matter Mater. Phys.* **2007**, *75*, 195410.
(45) Olmon, R. L.; Rang, M.; Krenz, P. M.; Lail, B. A.; Saraf, L. V.; Boreman, G. D.; Raschke, M. B. Determination of electric-field, magnetic-field, and electric-current distributions of infrared optical antennas: a near-field optical vector network analyzer. *Phys. Rev. Lett.* **2010**, *105*, 167403.

DOI: 10.1021/acsphotonics.6b00345
ACS Photonics 2016, 3, 1689−1697